IEEE Access
Multidisciplinary | Rapid Review | Open Access Journal

Received 13 May 2024, accepted 21 June 2024, date of publication 26 June 2024, date of current version 3 July 2024.

Digital Object Identifier 10.1109/ACCESS.2024.3419136

RESEARCH ARTICLE

Robust Sliding Mode Control for Time-Varying Systems With Adaptive Prescribed Performance

HONGJUN LI[1], SHENGJUN WEN[1], (Member, IEEE), JUN YU[1], AND HENGYI LI[2]
[1]Zhongyuan-Petersburg Aviation College, Zhongyuan University of Technology, Zhengzhou 450007, China
[2]Research Organization of Science and Technology, Ritsumeikan University, Kusatsu 525-8577, Japan

Corresponding author: Hongjun Li (li.hongjun@zut.edu.cn)

This work was supported in part by the General Project of the Natural Science Foundation in Henan Province under Grant 222300420595, in part by the Scientific and Technological Project in Henan Province under Grant 232102221035, and in part by the Key Research and Development Projects in Henan Province under Grant 231111221600.

ABSTRACT The system parameter variations will degrade the system performances, and they can not be estimated in time. This paper proposes a robust sliding mode control for time-varying systems with adaptive prescribed performance. Firstly, an adaptive prescribed performance function (PPF) is defined to overcome the singular problem that may occur in traditional PPFs. Based on the proposed PPF, the robust sliding mode control is proposed for systems with time-varying parameters. Instead of parameter estimation, their upper or lower bounds are used to design the controller. The system stability is analyzed by the Lyapunov function. Finally, the effectiveness of the proposed method is validated by simulations and experiments on a Peltier cooling system.

INDEX TERMS Prescribed performance function, sliding mode, time-varying systems.

I. INTRODUCTION

Many traditional controllers have been investigated for time-varying systems, such as PID [1], Neural Network [2]. For these conventional control methods, tracking error can converge to an unknown set or the maximum overshoot is unknown [3]. Prescribed performance control (PPC) is first introduced by Bechlioulis to ensure the tracking error has known bounds [4]. By defining prescribed performance functions (PPF), the tracking error will be restricted within pre-defined upper and lower bounds. Given a PPF, the maximum overshoot is less than the desired value, and the convergence rate is faster than the PPF.

The PPC has been applied to many control plants, such as quadrotors [5], dual-inertia driving systems [6] and synchronous traction systems [7]. The formulation of the PPF is important to the PPC. Most of the researchers use certain PPFs during the whole control process [8], [9], [10], [11], [12]. The drawback of this kind of PPF is that there will be a singular problem when the tracking error exceeds the desired bounds defined by PPFs. This problem will happen when the actual systems suffer uncertainty and disturbance [13]. What's more, the tracking error may exceed the PPF when the computed system input is outside the actuator's output range. In [13], the PPF changes once when the singular problem happens.

After defining a performance function, the transformed tracking error is without any constraints and the traditional controller can be applied. Neural networks are used to study the uncertain control plants in [14] and [15]. Fuzzy control is applied on nontriangular structure nonlinear systems in [16] and [17]. Adaptive control is used to tackle unknown input dynamics [18]. Some researchers also investigate sliding mode with PPFs to reduce the communication pressure of the central controller [19] or make the system converge rapidly in a finite time [20]. For nonlinear systems, [21] introduces a dynamic linearization technique for discrete-time nonlinear systems. Time-varying system parameters influence system stability and tracking performance. In [22], this kind of uncertainty is compensated for a free-flying space manipulator.

The associate editor coordinating the review of this manuscript and approving it for publication was Feiqi Deng.

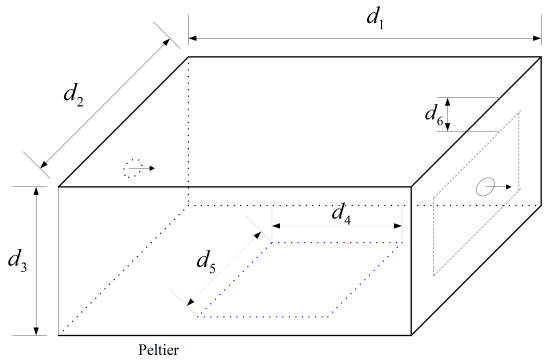

FIGURE 1. The configuration of the thermostat.

The estimated values of time-varying parameters are used to design the controller in [23] and [24].

In this paper, a robust sliding mode control with adaptive prescribed performance is proposed for time-varying systems. In order to avoid the singular problem in classical PPFs, an adaptive PPF changing with tracking error is developed, which is always larger than the tracking error. Based on the modified PPF, a new sliding mode surface is defined to design the controller. For time-varying systems, their parameters can not be estimated precisely in time when systems are suffering disturbance. A slide mode controller based on the sliding mode surface is developed without parameter estimation. The bounds of system parameters are used to design the controller. The main contributions of this paper are highlighted below.

(1) The proposal of an adaptive PPF. For traditional PPFs, the tracking error may exceed the pre-defined performance when systems suffer uncertainty and disturbance. This may cause a singular problem. In order to solve this problem, an adaptive PPF is defined, which can ensure that the tracking error is always within the bounds of the adaptive PPF.

(2) The proposal of a robust sliding mode control for a class of systems with time-varying parameters based on the proposed PPF. A new sliding mode surface based on the modified PPF is defined. Given the upper or lower bounds of system parameters, a sliding mode controller is proposed to ensure the system performance satisfies the predefined performance without parameter estimation.

The remainder part of this paper is organised as follows. Section II provides the time-varying model of the Peltier cooling system. In Section III, an adaptive PPF is presented. The robust sliding mode control based on the proposed adaptive PPF is shown in Section IV. The simulation and experimental results are given in Section V. The conclusions are provided in Section VI.

II. PELTIER COOLING SYSTEM

The proposed method will be applied to a Peltier cooling system which is shown in Figure 1. The Peltier is used to cool a thermostat where liquid flows in from the left side and out at a certain temperature. The sizes of the Peltier and thermostat are shown in Table 1.

TABLE 1. Parameters of the cooling system.

Symbol	Explanations
d_1	The outer length of thermostat
d_2	The outer width of thermostat
d_3	The outer height of thermostat
d_4	The length of Peltier
d_5	The width of Peltier
d_6	The thickness of thermostat

TABLE 2. Parameters of the peltier.

Symbol	Explanations
u	The voltage PWM duty cycle
I_c	The current
R_p	The Peltier resistance
S_p	The Seebeck coefficient
T_e	The endothermic side temperature
T_r	The radiation side temperature
K	The Peltier thermal conductivity
$k_1 - k_5$	Constants

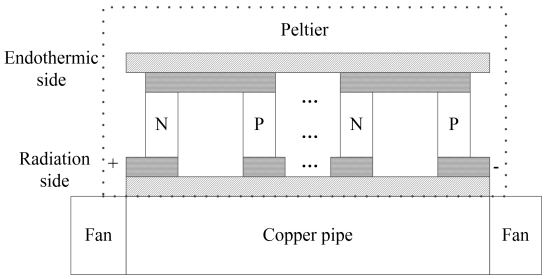

FIGURE 2. The peltier device.

The Peltier device is shown in Figure 2, which is controlled by voltage pulse width modulation (PWM). The endothermic side is used to cool the thermostat, and the heat radiates by copper pipe and fans from the other side. Its model consists of three parts: the Peltier effect, thermal conduction from the endothermic side to the radiation side, and the Joule heat by the current. As given in our previous work [25], the endothermic heat Q_p is given by

$$Q_p = (S_p T_1 I_c - \frac{1}{2} R_p I_c^2 + K k_1 I_c)u + K(k_2 e^{-k_3 t} - k_4 e^{-k_5 t}) \tag{1}$$

where the meaning of the variables in the above equation is shown in Table 2.

The Peltier device is at the bottom, and the heat of the thermostat is conducted from top to bottom. Besides liquid, there is also some air in the thermostat. The thermostat model consists of heat conduction, convective heat, and released heat of temperature decreases from thermostat, liquid and air. According to our previous work [25], this model is given by

$$\begin{aligned}(m_a c_a - m_l c_l - V_a c_v)\frac{\partial(T_0 - T(t))}{\partial t} \\ = -\lambda(T_0 - T(t))d_6\left(\frac{d_2}{d_1 - d_4 + 2d_3} + \frac{d_1}{d_3 + 2d_2}\right) \\ - \alpha(T_0 - T(t))d_4(d_2 - d_5) + Q_p\end{aligned} \tag{2}$$

TABLE 3. Parameters of the thermostat.

Symbol	Explanations
T_0	The initial temperature
$T(t)$	The current temperature
λ	Thermal conductivity of the thermostat
m_a	The quality of the thermostat
c_a	The specific heat coefficient of the thermostat
m_l	The quality of liquid in the thermostat
c_l	The specific heat coefficient of the liquid
V_a	Th air volume in the thermostat
c_v	The specific heat coefficient of air

The variable in the the above equation is explained in Table 3.

Define $y(t) = T_0 - T(t)$, and Equation (2) becomes

$$a_0' \frac{\partial y(t)}{\partial t} + a_1' y(t) = (S_p T_1 I_c - \frac{1}{2} R_p I_c^2 + K k_1 I_c)u + K(k_2 e^{-k_3 t} - k_4 e^{-k_5 t}) \tag{3}$$

where

$$a_0' = m_a c_a - m_l c_l - V_a c_v \tag{4}$$

$$a_1' = \lambda d_6 (\frac{d_2}{d_1 - d_4 + 2d_3} + \frac{d_1}{d_3 + 2d_2}) + \alpha d_4 (d_2 - d_5) \tag{5}$$

The liquid mass m_a and air volume V_a in the thermostat are time-varying. Heat radiation can be easily influenced by the surrounding environment. As a result, the system parameters are not constants. Define one time-varying variable β which satisfies

$$\beta u = K(k_2 e^{-k_3 t} - k_4 e^{-k_5 t}) \tag{6}$$

The thermostat model becomes

$$\dot{y}(t) + a_1 y(t) = b_1 u, \tag{7}$$

where

$$a_1 = a_1'/a_0' \tag{8}$$

$$b_1 = (S_p T_1 I_c - \frac{1}{2} R_p I_c^2 + K k_1 I_c + \beta)/a_0' \tag{9}$$

The two parameters a_1 and b_1 satisfy the following bounded condition:

$$|a_1| < \overline{a} \text{ and } 0 < \underline{b} < b_1 \tag{10}$$

The range of control input u is $[0\% - 100\%]$.

III. ADAPTIVE PRESCRIBED PERFORMANCE FUNCTION

Assuming the reference input is y_d, the tracking error is defined as

$$e(t) = y_d - y \tag{11}$$

According to the PPC theory, the tracking error $e(t)$ is always within a specified bound defined by a prescribed performance function. A typical prescribed performance function $e_m(t)$ is shown in Figure 3 where $e_{m,0}$ defines the maximum bound of overshoot and $e_{m,\infty}$ defines the maximum boundary of the

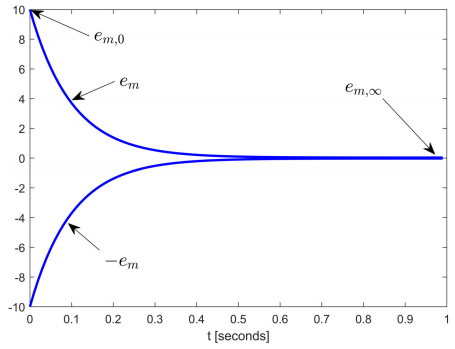

FIGURE 3. A prescribed performance function.

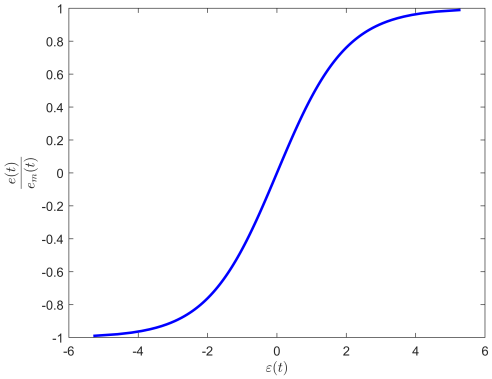

FIGURE 4. A transformation function.

tracking error at the steady-state. The PPC is to ensure the tracking error is always within the bound:

$$-e_m(t) < e(t) < e_m(t) \tag{12}$$

Normally, the PPF is given by

$$e_m(t) = (e_{m,0} - e_{m,\infty})\exp(-kt) + e_{m,\infty} \tag{13}$$

where $k > 0$ defines desired convergence rate of the tracking error and

$$0 < e_{m,\infty} < e_{m,0}$$
$$\lim_{t \to 0} e_m(t) = e_{m,0}$$
$$\lim_{t \to \infty} e_m(t) = e_{m,\infty}$$

Considering that it is difficult to directly design the controller under constraint (12), a smooth, strictly increasing function $\tau(\varepsilon)$ is introduced:

$$e = e_m \tau(\varepsilon) \tag{14}$$

where ε is the transformed error. The transformation function $\tau(\varepsilon)$ is strict increasing increase and satisfies:

$$\begin{cases} -1 < \tau(\varepsilon) < 1, \forall \varepsilon \\ \lim\limits_{\varepsilon \to -\infty} \tau(\varepsilon) = -1, \\ \lim\limits_{\varepsilon \to +\infty} \tau(\varepsilon) = 1, \\ \tau(\varepsilon) = 0. \text{ if } \varepsilon = 0 \end{cases} \tag{15}$$

The transform function $\tau(\varepsilon)$is selected as:

$$\tau(\varepsilon) = \frac{e^{\varepsilon} - e^{-\varepsilon}}{e^{\varepsilon} + e^{-\varepsilon}} \tag{16}$$

It is shown as Figure 4. The transformed error ε is given by

$$\varepsilon = \tau^{-1}(\frac{e}{e_m}) = \frac{1}{2}\ln(1 + \frac{e}{e_m}) - \frac{1}{2}\ln(1 - \frac{e}{e_m}) \tag{17}$$

When $e(t)$ is close to $e_m(t)$, the transformed error $\varepsilon(t)$ is close to ∞. When there is no disturbance in the actual systems, it can always be ensured that $|e(t)| < e_m(t)$. However, the disturbance in the actual systems are unavoidable. Especially in steady state, the system tracking error $e(t)$ may exceed the error bounds $(-e_m(t), e_m(t))$ when the actual system suffers disturbance. This will cause a singular problem. To avoid this problem, an adaptive prescribed performance function is proposed:

$$e_m(t) = |e(t)|\exp(-k(t - t_i)) + e_{m,\infty} \text{for } t \in [t_i, t_{i+1}) \tag{18}$$

where

$$\lim_{t \to t_i} e_m(t) = |e(t)| + e_{m,\infty} \tag{19}$$

Even though $|e(t)| > e_m(t)$ during time interval $[t_i, t_{i+1})$, the prescribed performance function will adapt quickly afterwords.

IV. SLIDING MODE CONTROL

The control task is to design a controller $u(t)$ so that the system output $y(t)$ can closely follow a reference signal $y_d(t)$. To design the sliding mode controller, a sliding variable s is defined as

$$s = \varepsilon \tag{20}$$

The derivative of the transformed error is computed as:

$$\dot{\varepsilon} = \frac{\partial \tau^{-1}}{\partial \frac{e}{e_m}}(\partial \frac{e}{e_m}) \tag{21}$$

$$= \frac{\partial \tau^{-1}}{\partial \frac{e}{e_m}} \frac{\dot{e}e_m - e\dot{e}_m}{e_m^2} \tag{22}$$

$$= \frac{\partial \tau^{-1}}{\partial \frac{e}{e_m}} \frac{1}{e_m}(\dot{e} - \frac{\dot{e}_m}{e_m}e) \tag{23}$$

$$= \frac{\partial \tau^{-1}}{\partial \frac{e}{e_m}} \frac{1}{e_m}(\dot{e} + \frac{(k|e| - |\dot{e}|)\exp(-k(t - t_i))}{e_m}e) \tag{24}$$

$$= v(\dot{e} + we) \tag{25}$$

where

$$w = \frac{(k|e| - |\dot{e}|)\exp(-k(t - t_i))}{e_m} \tag{26}$$

$$v = \frac{\partial \tau^{-1}}{\partial \frac{e}{e_m}} \frac{1}{e_m} \tag{27}$$

The derivative is computed as

$$\begin{aligned} \dot{s} &= \dot{\varepsilon} \\ &= v(\dot{e} + we) \\ &= v(\dot{y}_d(t) + a_1 y - b_1 u + we) \\ &= v(\dot{y}_d(t) + a_1 y + we - b_1 u) \end{aligned} \tag{28}$$

Assume the maximum of $\dot{y}_d$ is always not larger than a positive variable $\bar{\dot{y}}_d$, the controller is designed as follows:

$$u = u_1 + u_2 + u_3 \tag{29}$$

where

$$u_1 = \text{sgn}(s) \times \frac{\bar{\dot{y}}_d}{\underline{b}} \tag{30}$$

$$u_2 = \bar{a} \times \text{sgn}(s) \times \frac{|y|}{\underline{b}} \tag{31}$$

$$u_3 = \bar{w} \times \text{sgn}(s) \times \frac{|e|}{\underline{b}} \tag{32}$$

$$\bar{w} = \frac{(k|e(t)| + ||\dot{e}||)\exp(-k(t - t_i))}{e_m} \tag{33}$$

$$\text{sgn}(s) = \begin{cases} 1 & s > 0 \\ 0 & s = 0 \\ -1 & s < 0 \end{cases} \tag{34}$$

Here, $||\dot{e}||$ denotes the abstract of $|\dot{e}|$ and $\bar{w} > w$.

Theorem 1: Consider the time-varying system (7) with the control law (29) and adaptive prescribed performance function (18), the closed-loop control system is stable, and the tracking error e will converge to 0.

Proof: Designing the Lyapunov function as

$$V = s^2 \tag{35}$$

Take its time derivative and obtain

$$\begin{aligned} \dot{V} &= s\dot{s} \\ &= s(v(\dot{y}_d(t) + a_1 y + we - b_1 u_3)) \\ &= v((s\dot{y}_d(t) - sb_1 u_1) + (sa_1 y - sb_1 u_2) + (swe - sb_1 u_3)) \end{aligned}$$

The first term satisfies

$$\begin{aligned} s\dot{y}_d(t) - sb_1 u_1 &= s\dot{y}_d(t) - sb_1 \text{sgn}(s) \times \frac{\bar{\dot{y}}_d}{\underline{b}} \\ &= s\dot{y}_d(t) - |s|\frac{b_1}{\underline{b}}\bar{\dot{y}}_d \\ &\leq q|s|\bar{\dot{y}}_d - |s|\frac{b_1}{\underline{b}}\bar{\dot{y}}_d \\ &= (1 - \frac{b_1}{\underline{b}})|s|\bar{\dot{y}}_d \leqq 0 \end{aligned}$$

The second term satisfies

$$\begin{aligned} sa_1 y - sb_1 u_2 &= sa_1 y - sb_1 \bar{a} \times \text{sgn}(s) \times \frac{|y|}{\underline{b}} \\ &= sa_1 y - |s|\bar{a}\frac{b_1}{\underline{b}}|y| \\ &\leq q\bar{a}|s||y| - \bar{a}|s|\frac{b_1}{\underline{b}}|y| \\ &= (1 - \frac{b_1}{\underline{b}})\bar{a}|s||y| \leqq 0 \end{aligned}$$

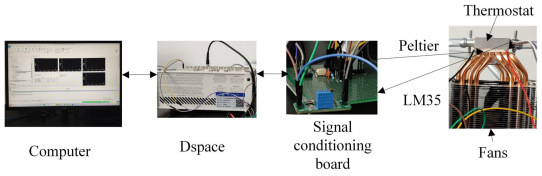

FIGURE 5. Block diagram of the experimental system.

The third term satisfies

$$\begin{aligned} swe - sb_1u_3 &= swe - sb_1\bar{w} \times \text{sgn}(s) \times \frac{|e|}{\underline{b}} \\ &= swe - |s|\bar{w}\frac{b_1}{\underline{b}}|e| \\ &\leq q\bar{w}|s||e| - \bar{w}|s|\frac{b_1}{\underline{b}}|e| \\ &= (1 - \frac{b_1}{\underline{b}})\bar{w}|s||e| \leqq 0 \end{aligned}$$

The variable v can be calculated as

$$v = \frac{\partial \tau^{-1}}{\partial \frac{e}{e_m}} \frac{1}{e_m} \tag{36}$$

$$= (\frac{1}{2}\frac{1}{1+\frac{e}{e_m}} - \frac{1}{2}\frac{-1}{1-\frac{e}{e_m}})\frac{1}{e_m} \tag{37}$$

$$= \frac{1}{2}(\frac{1}{1+\frac{e}{e_m}} + \frac{1}{1-\frac{e}{e_m}})\frac{1}{e_m} \tag{38}$$

$$= \frac{1}{1-(\frac{e}{e_m})^2}\frac{1}{e_m} \tag{39}$$

Because of the proposed adaptive prescribed performance function, the condition $-1 < \frac{e}{e_m} < 1$ can always be ensured. What's more, e_m is always positive and v is a positive variable. It means that $\dot{V} \leqq 0$. As a result, ε will converge to 0 and the system is stable. Based on the transformed function, the tracking error e will converge to 0. ■

V. SIMULATION AND EXPERIMENTAL RESULTS

A. EXPERIMENTAL SETUP

In the experiment, A LM35 temperature sensor is used and its voltage output is amplified by a signal conditioning board. A Dspace is used to collect temperature data and produce PWM. The PWM amplitude is converted from 5 V to 12 V by the signal conditioning board. A computer is used to program the Dspace and collect experimental data. The block diagram of the experimental system is shown in Figure 5.

B. SYSTEM PARAMETERS

The system outputs with different PWM duties are shown in Figure 6. Because of the low precision temperature sensor, the system output in the steady period with a constant input varies in 0.1 °C. When the PWM duty is more than 50, the temperature will be below 0 and the temperature sensor can not detect it. Because of this limitation, the response with higher PWM duty is not given here. The time constant and system gain for each system response are shown in Table 4.

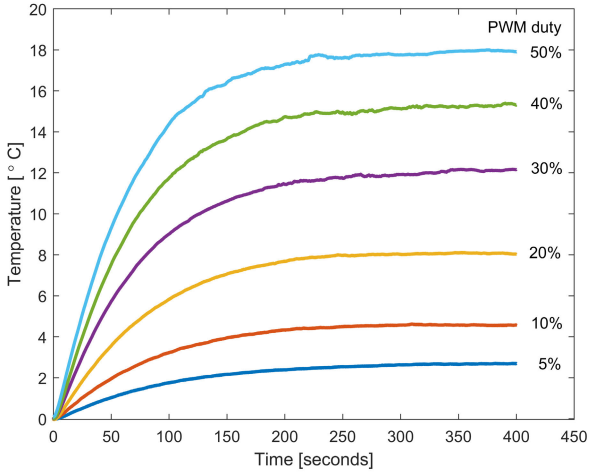

FIGURE 6. The system outputs with different PWM duties.

TABLE 4. Time constants and system gains for different system responses.

PWM duty	Time constant(s)	System gain
5%	89	0.53
10%	80	0.45
20%	78	0.4
30%	71	0.4
40%	67	0.38
50%	62	0.35

Based on these data, the range of a_1 is about 1/90-1/40 and the range of b_1 is about 0.004-0.005. In the following simulations and experiments, the parameters $\bar{a}$ and $\underline{b}$ are set to 0.025 and 0.005, respectively.

C. SIMULATION RESULTS

In this section, we provide some simulation examples to verify the efficiency of the proposed controller. The sampling time interval is 0.1 s. Based on the above ranges of two parameters a_1 and b_1, the system parameters are set to

$$a_1 = \frac{1}{65 + 25\sin(t)} \tag{40}$$

$$b_1 = 0.005 + 0.0005\sin(t) \tag{41}$$

as shown in Figure 7. The parameters k and $e_{m,\infty}$ are set to 1 and 0.03, respectively. The reference input is set to 10 and its maximum derivative $\bar{\dot{y}}_d$ is 0, and the system output and control input are shown as Figures 8. The system output becomes steady at 25 s. During the steady period, there is chatting and the maximum tracking error is about 0.02 °C. To test the proposed controller, an external disturbance with a value of -3 °C is added to the system output. The system entries the steady state in 9 s. The control input is shown in Figure 9. At the beginning, the control output is set to its upper bound for 23 s. If the Peltier has a more powerful cooling ability, the system can reach the steady state more quickly. During the steady period, the control output chatters. When the external disturbance appears, the controller adjusts quickly and the Peltier reaches its best cooling ability.

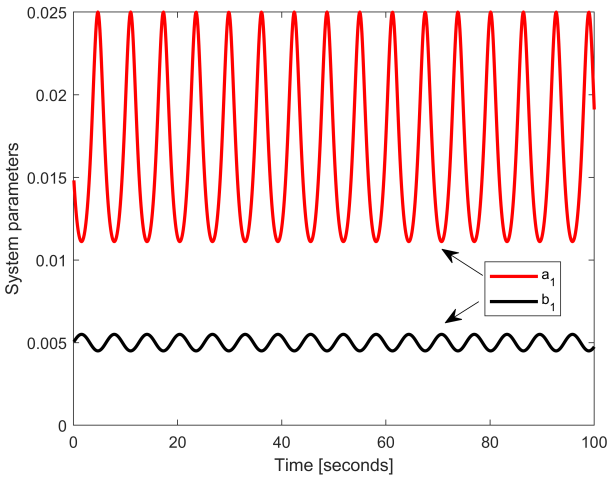

FIGURE 7. The variation of the system parameters.

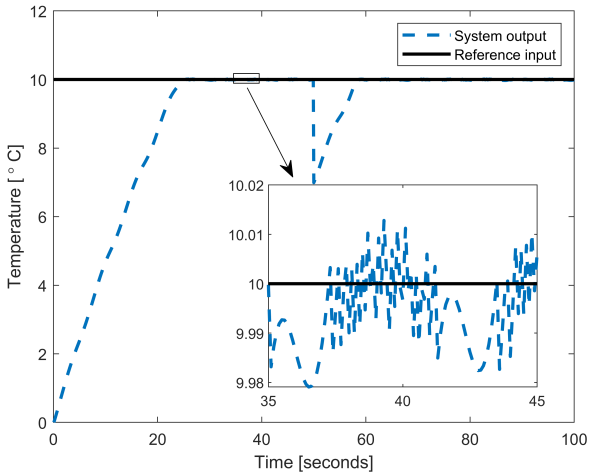

FIGURE 8. System output and reference input.

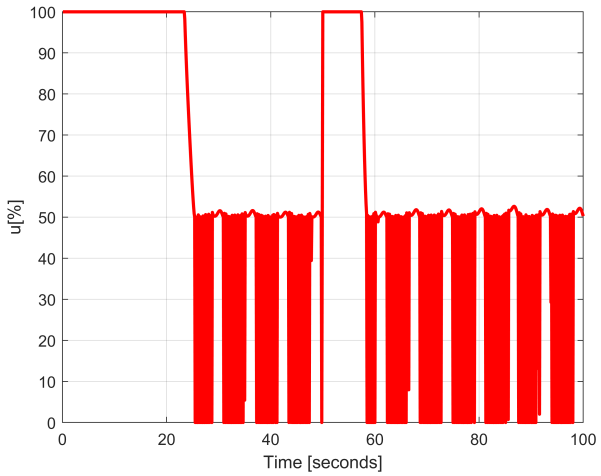

FIGURE 9. System input.

Figure 10 shows the tracking error and the proposed PPF, and there is also a traditional PPF whose formulation is $(5-0.03)\exp(-t)+0.03$. The tracking error is always within the bounds of the proposed PPF. In the tracking stage, the system outputs 100% for a long time, and the error exceeds

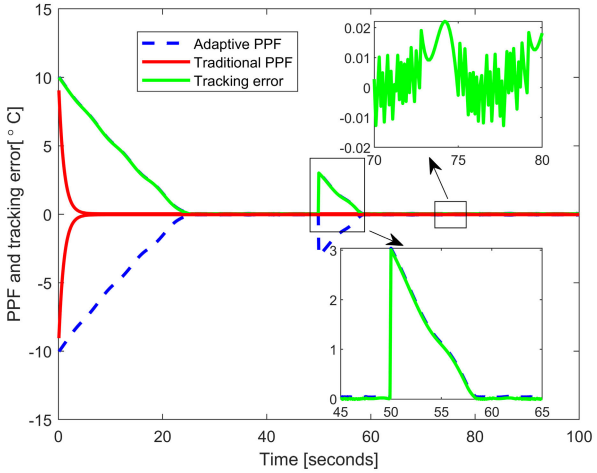

FIGURE 10. Tracking error and PPF.

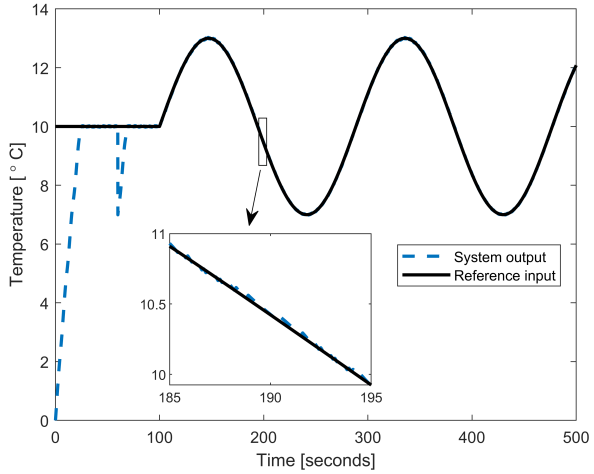

FIGURE 11. System output when the reference input changes.

the bound of the traditional PPF because of the cooling ability. Due to the external disturbance, the tracking error is outside of the restriction of the traditional PPF during steady periods.

In order to test the tracking ability, the reference input y_d changes as:

$$y_d = \begin{cases} 10, & 0\text{ s} < t < 100\text{ s} \\ 10 + 3\sin(\dfrac{t-100}{30}), & 100\text{ s} < t \end{cases} \tag{42}$$

Its maximum derivative $\bar{\dot{y}}_d$ is 1/10. The system parameters also vary as Figure 7. The system output and input are shown in Figure 11 and Figure 12, respectively. At the first period of the reference input, the system output is the same as shown in Figure 8. After that, the controller starts to track the sinusoidal reference input and the maximum tracking error is 0.04 °C.

The corresponding adaptive PPF and tracking error are shown in Figure 13. Even though the reference input is time-varying and there is an external disturbance, the error is never larger than the proposed PPF and the singular problem does not happen. It is also shown that the maximum tracking is about 0.04 °C for the sinusoidal reference input.

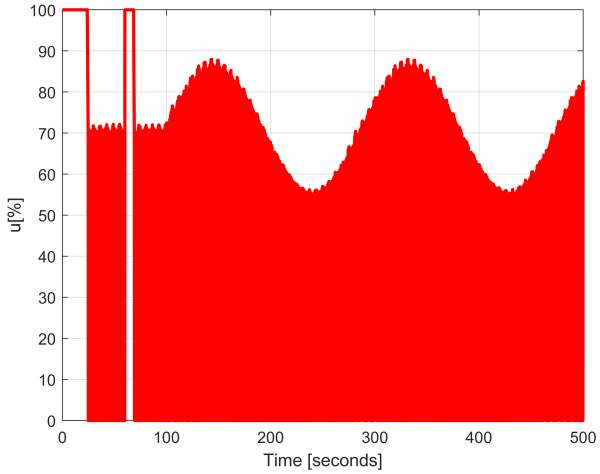

FIGURE 12. System input when the reference input changes.

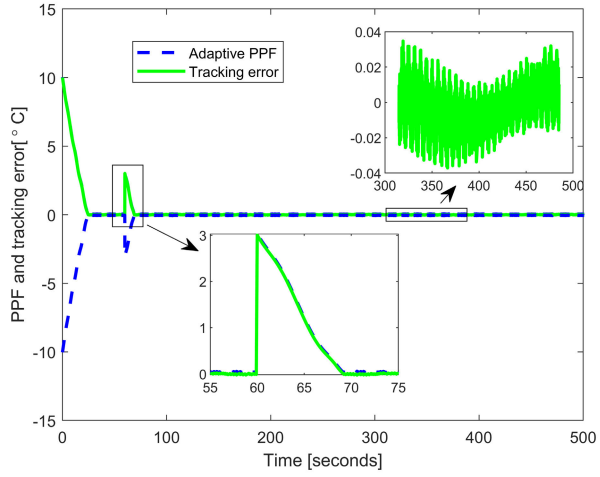

FIGURE 13. Tracking error when the reference input changes.

The proposed method is also compared with the widely used PID controller. The system parameters vary as Figure 7. The PID controller is described by

$$u_{pid} = K_P e(t) + K_I \int e(t) + K_D \dot{e}(t) \tag{43}$$

where $K_P = 500$, $K_I = 0.47$ and $K_D = 0.1$. The reference input changes as Equation (42). The system output is shown as Figure 14. The system becomes steady in 25 s. Because of time-varying system parameters, the steady error also changes with time and the maximum steady error is about 0.06 °C. When there is an external disturbance, the system enters the steady state again in 10 s. Compared with Figure 12, the tracking performance with sinusoidal reference input becomes worse. The detail is shown in Figure 15, and the maximum error of tracking sinusoidal input is about 0.13 °C.

D. EXPERIMENTAL RESULTS

Given the same parameter setup as the simulation, the experimental result of the proposed method is shown in Figure 17. The system output becomes steady at 25 s. The

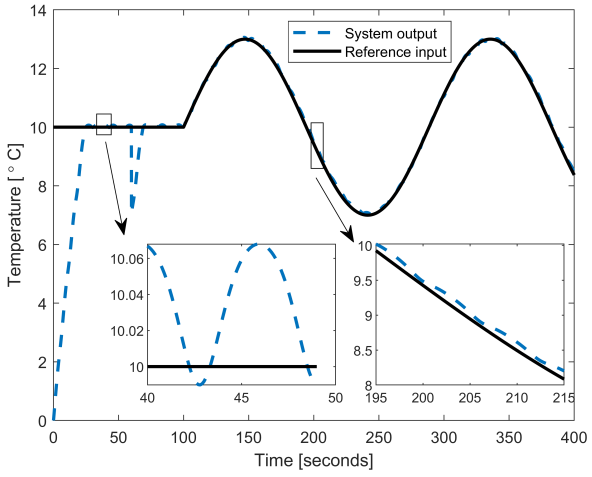

FIGURE 14. System output with PID controller.

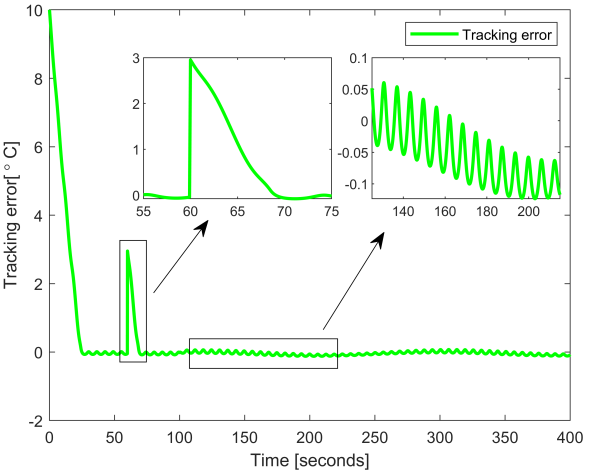

FIGURE 15. Tracking error of the PID controller.

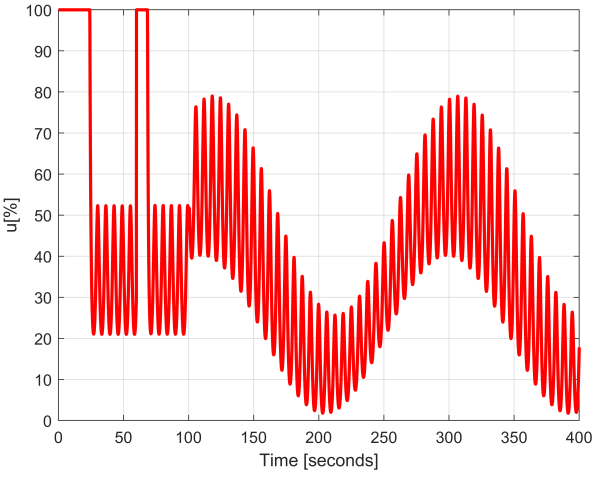

FIGURE 16. System input with PID controller.

maximum error during the steady and sinusoidal periods is 0.3 °C. The experimental result of the PID controller is shown in Figure 18. The system output becomes steady at 45 s and the maximum error during the steady and sinusoidal periods is 0.43 °C.

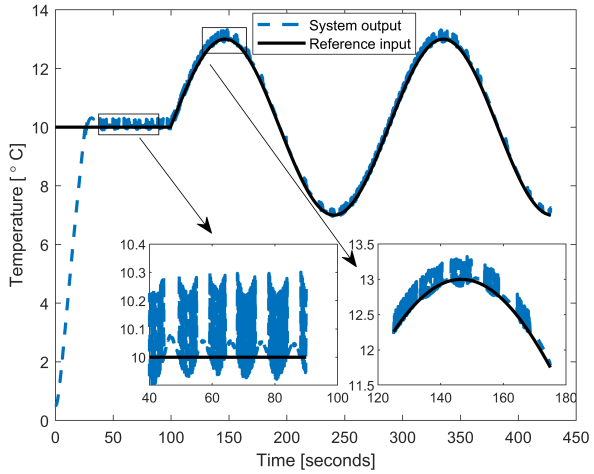

FIGURE 17. Experimental result of the proposed controller.

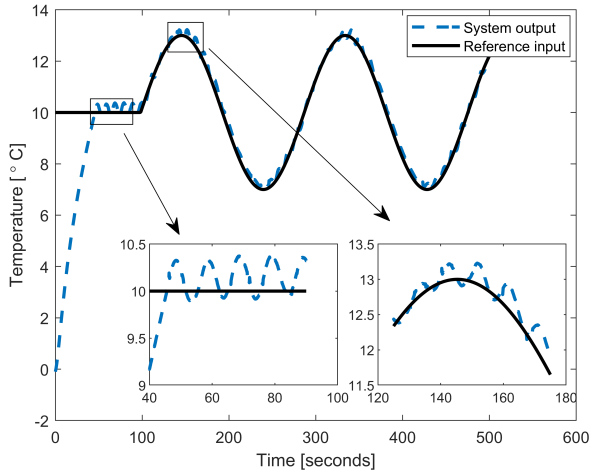

FIGURE 18. Experimental result of the PID controller.

E. DISCUSSION

From the simulation results, we know that the proposed PPF can avoid the singular problem that may happen when an external disturbance is added. Compared with the PID controller, the proposed method has smaller steady and tracking errors. Because of the low precision sensor in the experiments, Both the two methods have bigger errors in experimental results. The proposed method has the same setting time in the simulation and experiments. Meanwhile, the setting time of the PID controller becomes long in the experiments.

Because of the usage of the sign function sgn(s), there is chattering in the proposed method. The chattering can be avoided by using the function sgn(s) is replaced by a slop function in control law:

$$\text{sat}(s) = \begin{cases} s/\ell & |s| < \ell \\ \text{sgn}(s) & \text{else} \end{cases} \tag{44}$$

where ℓ is a constant. However, the steady error becomes larger when ℓ decreases as shown in Figure 19.

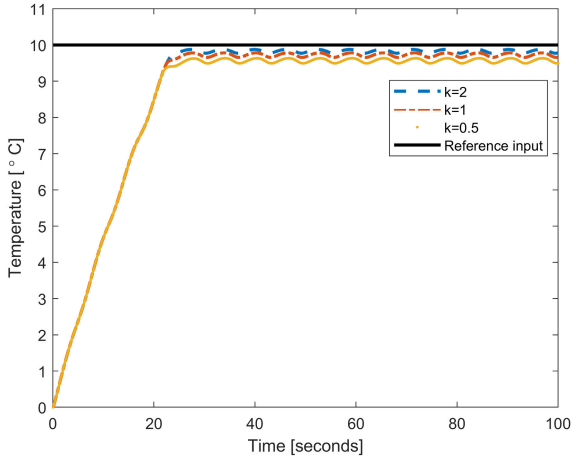

FIGURE 19. Simulation results of the proposed method with different ℓ.

VI. CONCLUSION

In this paper, a robust sliding mode control for time-varying systems with adaptive prescribed performance is proposed. The model of the Peltier cooling system is given with unknown parameters. An adaptive PPF associated with tracking error is proposed to tackle the singular problem. The sliding surface is designed based on the transformed error. Given the upper or lower bounds of system parameters, the robust sliding mode control is designed without parameter estimation. The simulation results show that the maximum steady-state error is 0.02 °C. The maximum tracking error for time-varying reference input is 0.04°C. In the experimental results, the maximum steady-state error and tracking error for the sinusoidal reference are 0.3 °C. Compared with the PID controller, the proposed method has a robust performance in experiments. The simulation and experimental results confirm the effectiveness of the proposed method. In the future, we intend to study how to overcome the chattering problem without decreasing system performance. After that, we will control the plant by a remote computer through the network and design a new sliding mode controller for the networked system.

REFERENCES

[1] J. Hao and G. Zhang, "Data-driven tracking control for a class of unknown nonlinear time-varying systems using improved PID neural network and cohen-coon approach," in *Proc. IEEE 10th Data Driven Control Learn. Syst. Conf. (DDCLS)*, May 2021, pp. 619–624.

[2] Y. Zhu, X. Li, H. Zheng, Z. Yang, Y. Wu, J. Fei, and Z. Fu, "Control of time varying nonlinear system of supporting robot based on neural network," in *Proc. 1st Int. Conf. Electron. Instrum. Inf. Syst. (EIIS)*, Jun. 2017, pp. 1–5.

[3] X. Bu, G. He, and D. Wei, "A new prescribed performance control approach for uncertain nonlinear dynamic systems via back-stepping," *J. Franklin Inst.*, vol. 355, no. 17, pp. 8510–8536, Nov. 2018.

[4] C. P. Bechlioulis and G. A. Rovithakis, "Robust adaptive control of feedback linearizable MIMO nonlinear systems with prescribed performance," *IEEE Trans. Autom. Control*, vol. 53, no. 9, pp. 2090–2099, Oct. 2008.

[5] G. Xu, Y. Xia, D. Zhai, and D. Ma, "Adaptive prescribed performance terminal sliding mode attitude control for quadrotor under input saturation," *IET Control Theory Appl.*, vol. 14, no. 17, pp. 2473–2480, Nov. 2020.

[6] S. Wang, J. Na, and Q. Chen, "Adaptive predefined performance sliding mode control of motor driving systems with disturbances," *IEEE Trans. Energy Convers.*, vol. 36, no. 3, pp. 1931–1939, Sep. 2021.

[7] B. Ding, D. Xu, B. Jiang, P. Shi, and W. Yang, "Disturbance-observer-based terminal sliding mode control for linear traction system with prescribed performance," *IEEE Trans. Transport. Electrific.*, vol. 7, no. 2, pp. 649–658, Jun. 2021.
[8] X. Bu, B. Jiang, and H. Lei, "Nonfragile quantitative prescribed performance control of waverider vehicles with actuator saturation," *IEEE Trans. Aerosp. Electron. Syst.*, vol. 58, no. 4, pp. 3538–3548, Aug. 2022.
[9] C. Wei, Q. Chen, J. Liu, Z. Yin, and J. Luo, "An overview of prescribed performance control and its application to spacecraft attitude system," *Proc. Inst. Mech. Eng. I, J. Syst. Control Eng.*, vol. 235, no. 4, Apr. 2021, Art. no. 095965182095255.
[10] T. N. Truong, A. T. Vo, and H.-J. Kang, "A model-free terminal sliding mode control for robots: Achieving fixed-time prescribed performance and convergence," *ISA Trans.*, vol. 144, pp. 330–341, Jan. 2024.
[11] M. L. Nguyen, X. Chen, and F. Yang, "Discrete-time quasi-sliding-mode control with prescribed performance function and its application to piezo-actuated positioning systems," *IEEE Trans. Ind. Electron.*, vol. 65, no. 1, pp. 942–950, Jan. 2018.
[12] C. Jing, H. Xu, and X. Niu, "Adaptive sliding mode disturbance rejection control with prescribed performance for robotic manipulators," *ISA Trans.*, vol. 91, pp. 41–51, Aug. 2019.
[13] J. Wang, J. Rong, and L. Yu, "Dynamic prescribed performance sliding mode control for DC–DC buck converter system with mismatched time-varying disturbances," *ISA Trans.*, vol. 129, pp. 546–557, Oct. 2022.
[14] S. Sui, C. L. P. Chen, and S. Tong, "A novel adaptive NN prescribed performance control for stochastic nonlinear systems," *IEEE Trans. Neural Netw. Learn. Syst.*, vol. 32, no. 7, pp. 3196–3205, Jul. 2021.
[15] Y. Li and S. Tong, "Adaptive neural networks prescribed performance control design for switched interconnected uncertain nonlinear systems," *IEEE Trans. Neural Netw. Learn. Syst.*, vol. 29, no. 7, pp. 3059–3068, Jul. 2018.
[16] Y. Li, X. Shao, and S. Tong, "Adaptive fuzzy prescribed performance control of nontriangular structure nonlinear systems," *IEEE Trans. Fuzzy Syst.*, vol. 28, no. 10, pp. 2416–2426, Oct. 2020.
[17] L. Zhang and G.-H. Yang, "Adaptive fuzzy prescribed performance control of nonlinear systems with hysteretic actuator nonlinearity and faults," *IEEE Trans. Syst., Man, Cybern., Syst.*, vol. 48, no. 12, pp. 2349–2358, Dec. 2018.
[18] X. Xia, T. Zhang, Y. Yi, and Q. Shen, "Adaptive prescribed performance control of output feedback systems including input unmodeled dynamics," *Neurocomputing*, vol. 190, pp. 226–236, May 2016.
[19] S. Huang, J. Wang, L. Xiong, J. Liu, P. Li, and Z. Wang, "Distributed predefined-time fractional-order sliding mode control for power system with prescribed tracking performance," *IEEE Trans. Power Syst.*, vol. 37, no. 3, pp. 2233–2246, May 2022.
[20] Y.-J. Liu and H. Chen, "Adaptive sliding mode control for uncertain active suspension systems with prescribed performance," *IEEE Trans. Syst., Man, Cybern., Syst.*, vol. 51, no. 10, pp. 6414–6422, Oct. 2021.
[21] M. Liu, Z. Zhao, and L. Hao, "Prescribed performance model-free adaptive sliding mode control of a shape memory alloy actuated system," *ISA Trans.*, vol. 123, pp. 339–345, Apr. 2022.
[22] Y. Zhu, J. Qiao, and L. Guo, "Adaptive sliding mode disturbance observer-based composite control with prescribed performance of space manipulators for target capturing," *IEEE Trans. Ind. Electron.*, vol. 66, no. 3, pp. 1973–1983, Mar. 2019.
[23] C. Lu and J. Fei, "Adaptive prescribed performance sliding mode control of MEMS gyroscope," *Trans. Inst. Meas. Control*, vol. 40, no. 2, pp. 400–412, Jan. 2018.
[24] G. Guo and D. Li, "Adaptive sliding mode control of vehicular platoons with prescribed tracking performance," *IEEE Trans. Veh. Technol.*, vol. 68, no. 8, pp. 7511–7520, Aug. 2019.
[25] H. Li, Y. Jin, P. Liu, J. Yu, R. Zhao, X. Yue, and S. Wen, "Adaptive model output following control for a networked thermostat," *Appl. Sci.*, vol. 12, no. 12, p. 6084, Jun. 2022.

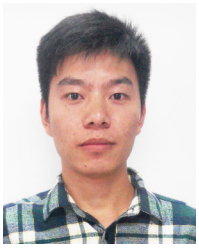

HONGJUN LI received the B.S. degree in communication engineering and the M.S. degree in control engineering from Zhongyuan University of Technology, Zhengzhou, China, in 2012 and 2015, respectively, and the Ph.D. degree in computer science from the University of Évora, Evora, Portugal, in 2019. He is currently with Zhongyuan-Petersburg Aviation College, Zhongyuan University of Technology. His research interests include adaptive control and SLAM.

SHENGJUN WEN (Member, IEEE) received the B.E. and M.Sc. degrees from the Department of Electrical Engineering, Zhengzhou University, China, in 2001 and 2004, respectively, and the Ph.D. degree in electronic and information engineering from the Graduate School of Engineering, Tokyo University of Agriculture and Technology, in 2011. He was a Visiting Fellow with the Shibaura Institute of Technology, Japan, from September 2018 to August 2019. He is currently an Associate Professor with Zhongyuan-Petersburg Aviation College, Zhongyuan University of Technology. He has authored or coauthored one book and more than 40 journal articles and 30 conference papers. His research interests include nonlinear control, adaptive control, fault diagnosis, and robotics. He received the Research Scholarship sponsored by the WESCO Scientific Promotion Foundation and the National Scholarship for Privately Financed International Students.

JUN YU received the Ph.D. degree in mechanical and electronic engineering from Nanjing University of Aeronautics and Astronautics, in 2012. He is currently with Zhongyuan-Petersburg Aviation College, Zhongyuan University of Technology. His research interests include robust control and bio-robot.

HENGYI LI received the Ph.D. degree in advanced electrical, electronic, and computer systems from Ritsumeikan University, Japan, in 2023. He is currently a Senior Researcher with the Research Organization of Science and Technology, Ritsumeikan University. His research interests include high-performance computing, computer architecture, deep learning, FPGA-based accelerator design for artificial intelligence (AI), and edge computing.